Energy & Environmental Science

ROYAL SOCIETY OF CHEMISTRY

PAPER

View Article Online
View Journal | View Issue

Cite this: *Energy Environ. Sci.*, 2026, **19**, 3021

Biphasic valorization of byproducts from biodiesel synthesis using floating photochemo-enzymatic domino catalysis

Andrea Rogolino and Erwin Reisner *

Sustainable chemical synthesis requires a cradle-to-cradle design strategy to upcycle waste streams with optimal atom and step economy. Here, we demonstrate the full valorization of vegetable oil using a scalable two-step process. First, transesterification of triglycerides (vegetable oil) with methanol in aqueous NaOH generates biodiesel, together with glycerol and unreacted unsaturated fatty acids as byproducts. Following separation of biodiesel, glycerol and fatty acids were valorized using a biphasic domino reaction at the liquid–liquid interface with a floating photochemo-enzymatic platform. Specifically, a floatable polymeric carbon nitride/polypropylene (CN_x/PP) composite photo-catalyzes first the reduction of O_2 to H_2O_2 using aqueous glycerol as the electron donor to produce glyceraldehyde and dihydroxyacetone. An immobilized lipase on a floating acrylic resin support subsequently utilizes the *in situ* generated aqueous H_2O_2 for the conversion of unsaturated fatty acids into epoxides in ethyl acetate. This novel photochemo-enzymatic domino reaction enables the full valorization of waste cooking oil at 1 kg scale, producing biodiesel (550 g), epoxidized fatty acids (438 g) and glyceraldehyde (663 g) in a 100 mL scale reactor under blue LED (λ = 450 nm, 40 $\pm$ 4 mW cm^{-2}) and simulated solar light (AM1.5G) at 40 °C generated by solar heating. A comparative life cycle assessment indicates that our integrated solar-driven process with optimized catalyst recyclability over 100 cycles has an expected 39% lower global warming potential compared to a decentralized process for conventional biodiesel, epoxy fatty acids and glyceraldehyde synthesis.

Received 10th December 2025,
Accepted 7th April 2026

DOI: 10.1039/d5ee07523h

rsc.li/ees

Broader context

Biodiesel synthesis from the transesterification of triglycerides from fatty waste such as vegetable cooking oil is the predominant industrial process for the generation of combustibles from plant-derived sewage, reaching 73 billion tons production in 2024. Despite the surging interest in the synthesis of renewable fuels, the valorization of the massive amounts of by-products of this process, namely glycerol and unreacted unsaturated fatty acids, has received little attention. Here, we provide a sustainable solution to this challenge and introduce a scalable and practical one-pot process for the full valorization of all biodiesel byproducts using recently emerged liquid|solid|liquid (L|S|L) photocatalysis. A visible light-absorbing polymeric carbon nitride (CN_x)/plastic composite and a lipase immobilized on acrylic resin float at the interface between hydrophilic glycerol and hydrophobic fatty acids. Simultaneous valorization of the byproducts proceeds through photocatalytic glycerol oxidation to glyceraldehyde coupled to oxygen reduction to hydrogen peroxide, which is in turn used *in situ* for the enzymatic conversion of fatty acids into epoxides relevant to the industry of polymers and plasticizers. Our study demonstrates full valorization of all biodiesel byproducts in flow liquid–liquid catalysis approaching kg scale with projected mitigated global warming potential compared to existing processes by a comparative life cycle assessment.

Introduction

The use of floatable photocatalysts on open water has recently emerged as an attractive approach in solar fuel production as it overcomes constraints from land usage, and it provides a means to easier catalyst recovery and enhanced photon utilization.[1] Although efforts have almost exclusively focused on the evolution of H_2,[2–5] or CO_2 reduction,[6,7] the concept holds particular potential for more diversified organic chemical synthesis. In particular, photocatalysts floating between two immiscible liquid phases open new possibilities for chemical conversion at the aqueous-organic interface.[8]

The macroscopic compartmentalization of chemical reactions between two liquid bulk phases takes inspiration from nanoscopic systems, often based on bio-mimetic micellar or

Yusuf Hamied Department of Chemistry, University of Cambridge, Lensfield Road, Cambridge CB2 1EW, UK. E-mail: reisner@ch.cam.ac.uk

liposomal assemblies,[9–12] or Pickering emulsions.[13–17] Examples of reactions accelerated in oil–water emulsions include CO_2 reduction,[10] glycerol etherification,[14] enzymatic esterification,[17] and epoxidation.[16] While the macroscopic separation between liquid phases offers advantages in terms of catalyst sequestration, substrate supply and product isolation, this configuration can suffer from a low surface/volume ratio and thus potential mass transfer limitations toward the catalytic center compared to the nanostructured biphasic assemblies. To offset this limitation, compartmentalized liquid|solid|liquid (L|S|L) systems can eliminate diffusion-limited catalysis if the substrates can be sourced at high concentration in green solvents or in pure form (*e.g.*, abundant waste or byproduct streams)[18] and the photocatalytic system becomes dominated by the catalytic turnover rather than mass transport.

Photocatalysis on floatable matrices has so far only taken advantage of one-step redox reactions to demonstrate the benefits from catalyst as well as substrate and product separation in different phases. At the liquid-gas interface, H_2 escapes as a gas and CO_2 utilization benefits from the direct interface with the reactive gas in the headspace, whereas the products from the oxidation of organic electron donors remain in solution.[2–5] We have recently demonstrated the application of a floatable photocatalyst at the liquid–liquid interface for the synthesis of hydrophobic biomass-derived organic oxidation products and hydrophilic hydrogen peroxide from the oxygen reduction reaction (ORR) accumulating in the organic phase and water, respectively.[8] This phase-segregated L|S|L reactor supported the spontaneous chemical separation of products, but also displayed limitations in performance compared to fully homogeneous counterparts.[19–21]

Beyond the compartmentalized supply of substrates and accumulation of products, floatable photocatalysis in liquid|liquid mixtures can in principle provide a unique platform for domino catalysis, leveraging on the interfacial utilization of *in situ* generated intermediates. In this scenario, a chemical intermediate generated in a first step at the liquid–liquid interphase can then be immediately used in a second interfacial reaction, benefiting from a high local concentration and thus preventing their dilution into the bulk of a liquid phase. Domino reactions also call for the synergistic activity of multiple catalysts to accelerate each individual chemical step, encouraging the search for catalytic abiotic and biotic materials floatable on water that could work in tandem.

Here, we introduce a photochemo-enzymatic domino valorization reaction through L|S|L photocatalysis enabled by floating (bio)catalysts at the interface of a liquid–liquid biphasic mixture. First, a water-floatable photocatalyst composite fabricated from inexpensive protonated polymeric carbon nitride (H-CN_x) and polypropylene (PP) promotes the photo-oxidative valorization of glycerol in water coupled to the reduction of O_2 to aqueous H_2O_2. This *in situ* generated H_2O_2 is then used as an intermediate for a perhydrolysis reaction catalyzed by commercially available *Candida antarctica* lipase B immobilized on a water-floatable acrylic resin (iCALB).[22–24] The enzymatic perhydrolysis transfers one oxygen atom from aqueous H_2O_2 to unsaturated fatty acids in ethyl acetate, which are in turn converted into peroxy acids. Peroxy acids then generate epoxides through a conventional Prilezhaev reaction. The glycerol oxidation products glyceraldehyde and dihydroxyacetone are relevant to carbohydrate synthesis and the cosmetics industry,[25,26] whereas epoxidized fatty acids have emerged as a new class of monomers for the synthesis of biodegradable

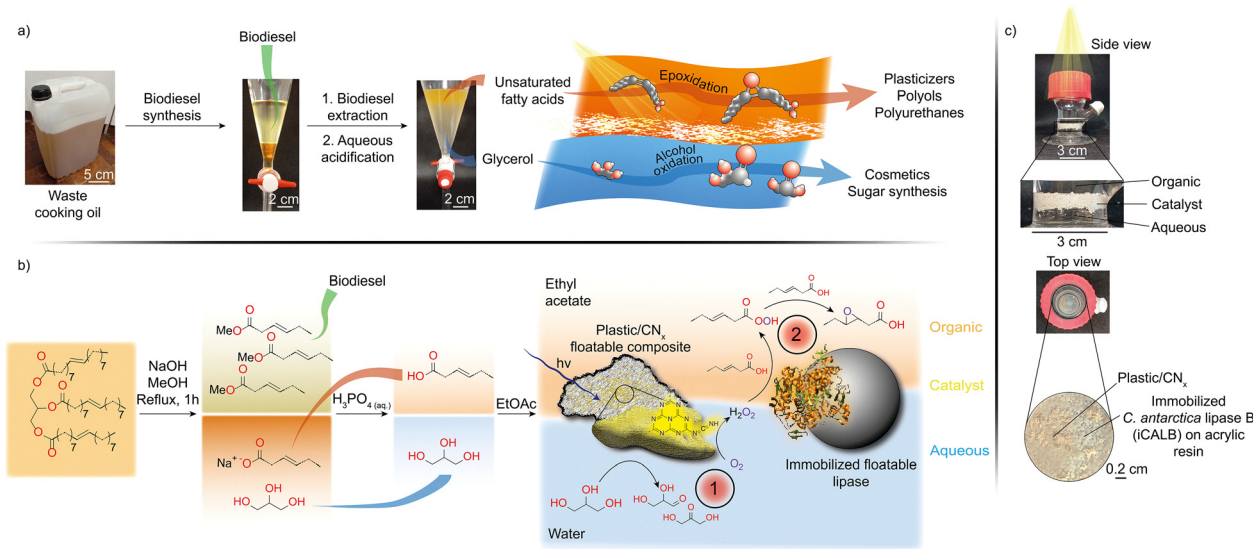

Fig. 1 (a) Illustration and (b) reaction scheme of vegetable oil fractionation and the L|S|L system for the simultaneous synthesis of added-value aqueous glyceraldehyde and dihydroxyacetone and organic epoxidized unsaturated fatty acids addressing the full valorization of fatty waste. (c) Side-view (top) and top-view (bottom) pictures of the custom top-down photoreactor, with close-ups of the L|S|L system (top) and the floatable catalysts (bottom).

plasticizers, polyols and polyurethanes.[27,28] Unsaturated fatty acids are also available in large quantities from tall oil, a byproduct of the Kraft pulp industry.[29] To demonstrate the full valorization of waste vegetable oils in an applied scenario (Fig. 1), we source fatty acids and glycerol as byproducts from biodiesel synthesis[30] and operate biodiesel synthesis and the fractionation of products with 1 kg vegetable oil as substrate, and byproduct valorization on a 100 mL scale. Photocatalysis succeeded under both simulated AM1.5G and natural sunlight using a custom flow photoreactor to allow independent transport and collection of both liquid phases. Finally, we present a life cycle assessment and simplified technoeconomic analysis to probe the industrial potential of L|S|L photocatalysis for centralized biodiesel synthesis, fatty acids and glycerol upcycling compared to existing protocols.

Results and discussion

Design and synthesis of floatable photocatalyst

The floatable photocatalysts were fabricated following a solvent-free protocol as previously reported.[8] Briefly, polymeric carbon nitride (CN_x) was prepared by thermal polymerization of melamine and post-functionalization with potassium thiocyanate. CN_x powder and finely ground amorphous polypropylene were mixed under cryogenic cooling (77 K) in 6 : 4 (w/w) ratio. The solid blend was stirred at 120 °C for ~15 min to partially melt the plastic and yield the photocatalyst/plastic composite (CN_x/PP). The fraction floating on water was then recovered in a separatory funnel, yielding floatable composites with a typical density of 0.9 mg mL^{-1}.[8]

CN_x was chosen as a metal-free, inexpensive, non-toxic, and visible light-absorbing photocatalyst. CN_x-based materials also stand out for their high activity and selectivity in light-driven O_2-to-H_2O_2 reduction, outperforming alternatives mostly based on metal–organic frameworks (MOFs) and covalent organic frameworks (COFs).[31,32] CN_x photocatalysts with benchmark H_2O_2 production rate were initially screened in dispersion in the presence of alcohols as electron donors, including unmodified polymeric carbon nitride and poly(heptazine imides) synthesized by ionothermal synthesis or post-functionalization (Fig. S1).[19–21,33,34] In standard experimental conditions, the dispersed photocatalysts (5.0 mg in 2 mL 50 wt% aqueous glycerol) were irradiated with a blue LED (λ = 450 nm, 40 ± 4 mW cm^{-2}) in O_2-saturated atmosphere in a sealed vessel at 25 °C in a 11.5 mL glass vial (∅ = 2 cm, total volume: 11.5 mL). H_2O_2 was quantified colorimetrically using the titanium(IV) oxide oxalate method.[35]

Among all photocatalysts studied, CN_x obtained by post-functionalization of unmodified polymeric carbon nitride with potassium thiocyanate and protonated by the addition of aqueous 37 wt% hydrochloric acid (1 mL per 100 mg of material) (H-CN_x) achieved the highest photocatalytic H_2O_2 evolution rate (10.8 ± 0.6 mmol L^{-1} h^{-1}) and a seven-fold improvement compared to the unprotonated counterpart (K-CN_x) (1.5 ± 0.2 mmol L^{-1} h^{-1}). An increased activity in photocatalytic ORR with protonated poly(heptazine imides) was previously reported, although not fully rationalized.[34] Spectroscopic characterization and catalytic control studies suggest that the promoting activity of H-CN_x is merely a result of *in situ* acidification, lowering the pH of the aqueous medium to 4–5, and thereby suppressing H_2O_2 decomposition in neutral and alkaline solutions.[36–38] A more detailed investigation is discussed in Supplementary Note 1 (Fig. S2–S5 and Tables S1–S4).

The floatable enzymatic catalyst is a formulation commercially known as "Novozym 435", consisting of *Candida antarctica* lipase B expressed in *Aspergillus niger*, and immobilized on an acrylic resin support, with a reported activity of 5000 propyl laurate units (PLU) g^{-1} (see Supplementary Methods for detailed definition).

Photocatalytic H_2O_2 generation with glycerol valorization

The photochemo-enzymatic domino epoxidation was first studied by optimizing the individual reactions, namely (1) the photocatalytic ORR coupled with glycerol oxidation reaction (GOR), and (2) the iCALB-catalyzed perhydrolysis for the oxidation of unsaturated fatty acids to peroxy acids, followed by the chemical Prilezhaev epoxidation of the alkene (Fig. 1b). Highly concentrated aqueous glycerol (5–50 wt%) was used to prevent mass transfer limitations arising from electron donor diffusion to the floating photocatalyst. Samples with such a high glycerol concentration can be sourced from the biodiesel synthesis of waste cooking oil (116 g of glycerol from 1 kg of oil, Table 1).

We first assessed the lowest aqueous glycerol concentration needed to achieve the maximum photocatalytic H_2O_2 production rate in the presence of H-CN_x under the standard experimental conditions as above. A plateau in H_2O_2 evolution was reached with glycerol content of 30 wt%, giving a maximum rate of 12.8 ± 0.3 mmol L^{-1} h^{-1} (Fig. 2a). H_2O_2 and glyceraldehyde were also produced in comparable molar amounts within 1 h irradiation (26.0 ± 10.8 and 29.5 ± 4.6 mmol L^{-1}, respectively), confirming a stoichiometric $2H^+$-$2e^-$ redox process for both reactions (Table S5). Dihydroxyacetone was

Table 1 Recovered glycerol, fatty acids, and biodiesel fractions from vegetable oils[a]

Vegetable oil	Starting mass (g)	Methanol mass (g)	Recovered fraction (wt%)		
			Glycerol	Fatty acids	Biodiesel
Rapeseed	92.6	25.2	6.4	9.6	55.5
Sunflower	35.5	7.5	7.4	3.6	14.2
Olive	36.6	7.5	5.5	2.5	28.1
Soybean	37.1	7.5	9.9	10.4	27.7
Palm	40.0	7.5	2.7	2.6	24.6
Used vegetable oil	1000	230	11.6	9.0	55.0

[a] Biodiesel was first synthesized by stirring the mixture of vegetable oil and methanol with 0.9 wt% NaOH under reflux for 1 h. The biodiesel fraction was separated, and the glycerol phase was washed with ethyl acetate (3 × 10 mL). The collected glycerol phase was then acidified with H_3PO_4 (85 wt%) until pH ~2. The unreacted fatty acids fraction partitioning at the top was then separated and the glycerol phase was washed with ethyl acetate (3 × 10 mL). The glycerol phase was thus collected. Volatiles in the unreacted fatty acids fraction were removed under reduced pressure.

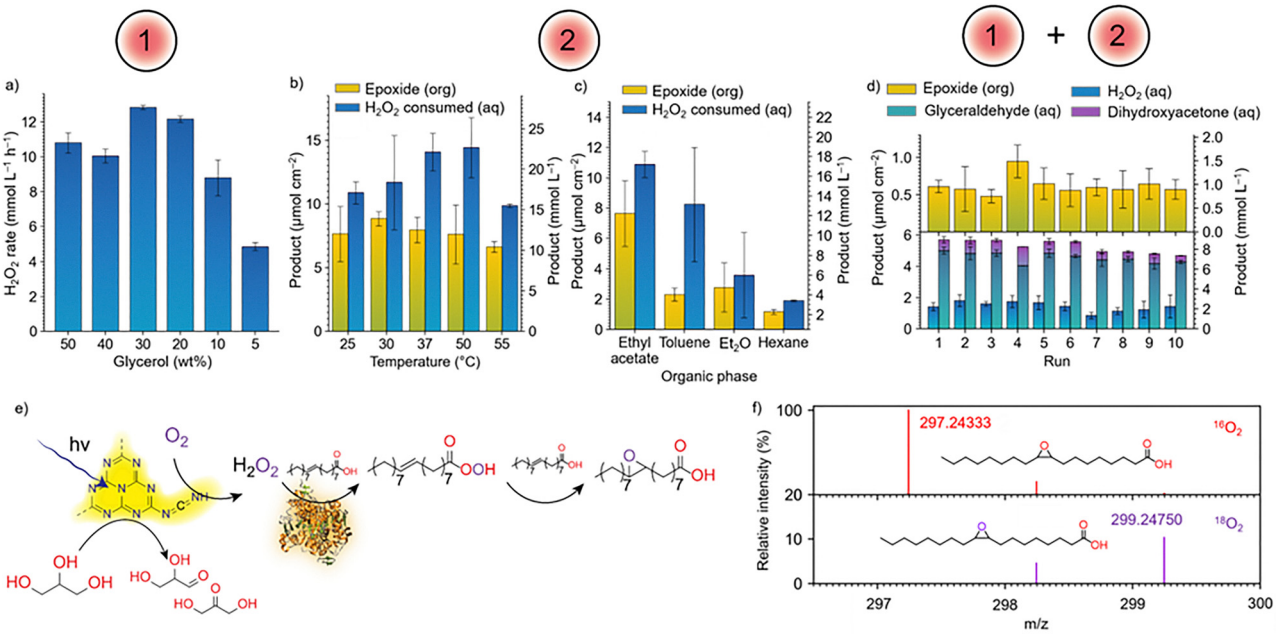

Fig. 2 Optimization of (a) glycerol concentration for photocatalytic H_2O_2 production, (b) temperature for enzymatic oleic acid epoxidation, (c) organic solvent for enzymatic oleic acid epoxidation. (d) Recyclability of the whole photochemo-enzymatic system for domino oleic acid epoxidation. Reaction conditions: a) aqueous glycerol (2 mL), H-CN_x (5 mg), O_2 (1 atm), 450 nm (40 ± 4 mW cm^{-2}), 25 °C. (b) Aqueous H_2O_2 (40 mM, 2 mL), iCALB (10 mg), oleic acid in ethyl acetate (40 wt%, 2 mL), 16 h. (c) Aqueous H_2O_2 (40 mM, 2 mL), iCALB (40 mg), oleic acid in organic solvent (40 wt%, 2 mL), 25 °C, 16 h. (d) Aqueous glycerol (30 wt%, 2 mL), oleic acid in ethyl acetate (40 wt%, 2 mL), H-CN_x/PP (20 mg), iCALB (40 mg), O_2 (1 atm), 450 nm (40 mW cm^{-2}), 25 °C, 2 h per run. Both liquid phases were removed and replaced after every run with needles, whereas the solid catalysts were reused. Numbers above the plots indicate the individual light-driven (1) and enzymatic (2) steps of the reaction, and the integrated domino (1 + 2), as illustrated in Fig. 1b. (e) Scheme of the photochemo-enzymatic domino epoxidation of oleic acid, showing O insertion from gaseous O_2 to the epoxide ring of 8,9-epoxystearic acid. (f) Accurate mass spectra of LC-MS analysis of 8,9-epoxystearic acid generated by photochemo-enzymatic domino reaction in the presence of $^{16}O_2$ (top) and $^{18}O_2$ (bottom). The data are presented as mean values ± standard deviation (error bars) for reactions performed in triplicate (n = 3).

produced in lower amounts and only observed at prolonged reaction times, as discussed below. Furthermore, O_2 availability was found to be an important parameter for prolonged ORR, with H_2O_2 generation increasing by a factor of 1.5 with multiple compared to single O_2 purging, indicating the depletion of the gas during the reaction (Fig. S6).

Enzymatic iCALB-catalyzed epoxidation with H_2O_2

Following the optimization of photocatalytic H_2O_2 production, we assessed first the possibility to target high alkene conversions in the organic phase in the presence of iCALB and aqueous H_2O_2 solutions in the dark. iCALB-catalyzed epoxidation of alkenes with H_2O_2 has been reported in several scenarios, targeting unsaturated fatty acids as organic substrates.[23,24,39–42] The mechanism of the epoxidation of oleic acid is generally acknowledged to proceed *via* the formation of the intermediate epoxidizing agent peroxyoleic acid *via* perhydrolysis (O atom transfer from H_2O_2 to the acid) catalyzed by the immobilized lipase. Peroxyoleic acid is then expected to transfer an oxygen atom to the unsaturation of the fatty acid, generating the epoxide.[43]

Preliminary tests were performed using *cis*-cyclooctene as a model alkene. Under these conditions, ethyl acetate itself can participate as a substrate for enzymatic hydrolysis into acetic acid and ethanol, generating peracetic acid as the final epoxidizing agent.[39] The active role of ethyl acetate in the domino reaction is discussed in more detail in Supplementary Note 2. The reaction was run at a scale of 0.2 mmol (22 mg) of *cis*-cyclooctene. With 40 mg iCALB in a 2 mL|2 mL ethyl acetate|water mixture at 40 °C, at least 10 equiv. of H_2O_2 (1000 mM) were needed to achieve >90% conversion of the alkene to the epoxide in 16 h (Fig. S7a). Decreasing the volumes of both the organic and aqueous solvents to increase the surface/volume ratio and enhance mass transfer between the two phases did not significantly improve the conversion (Fig. S7b). Vigorous shaking did also not improve yields significantly (Fig. S7b). While reaching such a high concentration of H_2O_2 is unrealistic for photocatalytic *in situ* production in the bulk, we hypothesize that it could be approached as a local concentration in proximity of the floating photocatalyst (see below).

We decided to use an excess of substrate in the organic phase to achieve high epoxidation rates rather than high yields. As for glycerol utilization in the aqueous phase, this choice is justified by the high amount of unsaturated fatty acids that can be obtained from waste vegetable oils and tall oils. The substrate concentration in the organic phase was also screened. As expected, higher volume fractions of the substrate in ethyl acetate resulted in higher epoxide production, and the organic substrate concentration did not affect glyceraldehyde and dihydroxyacetone distribution from GOR in the aqueous phase, as

determined by high-performance liquid chromatography (HPLC).

We then optimized the enzymatic step of the domino reaction using oleic acid as one of the most common unsaturated fatty acids found in vegetable oils. Epoxidized oleic acid (*cis*-8,9-epoxystearic acid) was monitored and quantified by nuclear magnetic resonance spectroscopy (quantitative ^{1}H-NMR, $CDCl_3$) by following the characteristic multiplet signal at 2.9 ppm belonging to the aliphatic protons of the epoxide ring (Fig. S8).[23,24] For clarity, epoxide yields are henceforth reported as variations (ΔProduct) from the background amount of epoxide naturally present in oleic acid (<0.5 mmol L^{-1}). Based on the screening of *cis*-cyclooctene optimized for epoxidation yields and substrate utilization (Fig. S6c), we selected a concentration of 40 wt% of oleic acid in ethyl acetate. Standard conditions for enzymatic epoxidation included aqueous H_2O_2 (40 mM, 2 mL), iCALB (40 mg), and oleic acid (40 wt% in 2 mL ethyl acetate) at 40 °C for a 16 h reaction. Temperature-dependent screening resulted in an optimal epoxidation yield (average: 7.8 ± 1.7 μmol cm^{-2}, normalized by the liquid–liquid interfacial area, or 12.2 ± 2.7 mmol L^{-1}, normalized by the volume of the bulk liquid phase) and H_2O_2 utilization (average: 14.2 ± 1.9 μmol cm^{-2}, 22.2 ± 3.0 mmol L^{-1}) between 37 °C and 50 °C (Fig. 2b), which is consistent with 40 °C being reported as the optimal temperature for iCALB activation.[44] This moderate temperature is also easily accessible by solar heating, thus enabling UV-vis light utilization for the photocatalytic reaction and infrared heating for the iCALB-catalyzed epoxidation.[45]

We subsequently screened various organic solvents to assess their role in the reaction. iCALB displays high stability in a range of water-immiscible organic solvents with density lower than water (1 g mL^{-1}), including ethyl acetate, toluene, diethyl ether (Et_2O), and hexane.[22,39] Screening runs under the standard conditions for enzymatic epoxidation and at room temperature (25 °C) resulted in ethyl acetate yielding the highest epoxidation yield of 7.6 ± 2.2 μmol cm^{-2} (11.9 ± 3.4 mmol L^{-1}), with a corresponding H_2O_2 consumption of 10.9 ± 0.9 μmol cm^{-2} (17.1 ± 1.4 mmol L^{-1}) (Fig. 2c). For all solvents, a correlation between epoxide production and H_2O_2 consumption was found, confirming the utilization of hydrogen peroxide as a stoichiometric reactant for the enzyme-catalyzed alkene epoxidation. The superior performance of ethyl acetate over other organic solvents for iCALB-catalyzed epoxidation has previously been reported (see Supplementary Note 2 for further discussion, Fig. S9 and S10).[39] The loading of iCALB was also optimized, with the epoxidation yield saturating at a mass of 9.6 mg cm^{-2} of the immobilized enzyme (522 ± 117 $\mu mol_{epoxide}$ cm^{-2} g^{-1}_{iCALB}) (Fig. S11).

Exclusion control experiments

Exclusion control experiments without photocatalyst, irradiation, enzyme or glycerol confirmed the essential role of the individual components for the photochemo-enzymatic domino reaction (Tables S6 and S7). Notably, using either non-immobilized (soluble) lipase or dispersed H-CN_x led to a decrease of epoxide production (8.9-fold and 1.5-fold, respectively), indicating the fundamental role of catalyst confinement at the interface (Table S6). Indeed, existing immobilization strategies including packed bed flow reactors,[46] photosheets or panels,[47,48] or coated reaction walls[49] would leave most of the catalyst far from the reactive region at the liquid–liquid boundary, and thus inactive.

Integrated L|S|L domino valorization

After establishing the optimized conditions for both parts of the photochemo-enzymatic domino reaction, we studied the activity of the fully integrated system over multiple recyclability cycles. Reactions were executed in a mixture of 30 wt% glycerol in 2 mL of water, 40 wt% oleic acid in 2 mL ethyl acetate, 20 mg of floatable H-CN_x/PP and 40 mg of iCALB, in O_2-saturated atmosphere in a sealed vessel under blue LED irradiation (λ = 450 nm, 40 ± 4 mW cm^{-2}). After each two-hour run, both liquid phases were removed with a needle, whereas the solid catalysts remained, and fresh solutions were added to the reaction flask. The whole system exhibited excellent recyclability, with an average glyceraldehyde and dihydroxyacetone production of 4.6 ± 0.3 μmol cm^{-2} (7.2 ± 0.5 mmol L^{-1}) and 0.7 ± 0.2 μmol cm^{-2} (1.1 ± 0.4 mmol L^{-1}) in the aqueous phase, and 0.62 ± 0.12 μmol cm^{-2} (0.97 ± 0.20 mmol L^{-1}) epoxide in the organic phase (Fig. 2d).

The same robustness was observed in a test under continuous operation over 6 days (Table S8). Here, the liquid phases were removed after 3 days, 40 mg additional iCALB were transferred to the vial to compensate for partial enzyme deactivation, whereas no fresh H-CN_x/PP was added. Again, no loss in performance was observed. Instead, the epoxide produced in the second 3-day run (62.7 ± 4.7 mmol L^{-1}) was ~1.6 times higher than in the first 3-day run (38.7 ± 5.0 mmol L^{-1}), indicating that the integration of more lipase after the first run was likely unnecessary.

Epoxides were produced with an external quantum efficiency (EQE) of 0.40 ± 0.31% under 420 nm irradiation. The L|S|L system preserved good macroscopic phase segregation even after 10 catalytic cycles (Fig. S12). Finally, we observed that fine grinding of the floatable CN_x/PP composite was crucial to achieve improved performance, since the activity of the H-CN_x/PP composite is determined by the amount of photocatalyst exposed on the surface. Particles were reduced to 0.1–0.5 cm in size by cryogenic cooling under liquid N_2 followed by mechanical grinding (Fig. S13). The same mass of H-CN_x resulted in a 3.8-fold increase in epoxide yield when used as fine particles as opposed to as-fabricated coarse flakes (1.49 ± 0.15 mmol L^{-1} and 0.39 ± 0.06 mmol L^{-1} over 2 h operation, respectively, Table S9). The observation underscores that accurate grinding is recommended for future applications of our proposed floatable composite.

The domino reaction starting from gaseous O_2 to oxygen insertion into an epoxide ring (Fig. 2e) has only been shown with anthraquinone as stoichiometric reductant for the Pd-catalyzed O_2-to-H_2O_2 reduction,[50] mimicking the conditions of industrial H_2O_2 synthesis,[51] followed by iCALB-catalyzed epoxidation. Nevertheless, the proposed oxygen atom insertion from

gaseous O_2 into the epoxide has not been experimentally validated. To track the fate of the oxygen atom from gas phase O_2 to the epoxide ring of *cis*-8,9-epoxystearic acid, we performed isotopic labelling tests using $^{18}O_2$. The photochemo-enzymatic reaction was run under the usual conditions feeding the headspace of the reaction vial either with O_2 of natural abundance or $^{18}O_2$ (97 atom%). The organic phase was analyzed by liquid chromatography-mass spectrometry (LC-MS) for accurate molecular mass determination, targeting epoxidized oleic acid. Isotopically labelled *cis*-8,9-epoxystearic acid (molecular mass: 299.24750 Da) was successfully detected only in the presence of $^{18}O_2$, with a *m/z* shift of 2.00417 Da from the same molecule detected with $^{16}O_2$ of natural abundance (297.24333 Da) (Fig. 2f and Table S10).

LC-MS measurements were also performed to detect the putative intermediate peroxyoleic acid, which was tentatively identified by tandem MS-MS spectrometry to distinguish it from its isomer 8,9-epoxystearic acid (Fig. S14). Fragmentation patterns suggested the presence of both the epoxide and the peracid in the organic mixture recovered after the photochemo-enzymatic reaction. Although the evidence is not conclusive to confirm the generation of the peracid, we believe that our findings present the first attempt to shed light on the mechanism of CALB-catalyzed epoxidation.[22,43]

Solar-driven domino valorization using L|S|L platform

To transfer the photochemo-enzymatic system to an outdoor application scenario, we also performed photocatalytic tests with simulated solar light irradiation under the same conditions as for the studies above using monochromatic light. The studies were performed in a custom glass reactor ($\varnothing$ = 3 cm, total volume: 50 mL) designed for top-down irradiation (Fig. 1c) with AM1.5G irradiation (100 mW cm^{-2}, 1 sun). A 400 nm cutoff filter was placed on the top of the reactor to prevent H_2O_2 decompositon. Due to the limited utilization of the solar spectrum given by the H-CN_x bandgap cutoff at ~430 nm (Fig. S2e), solar-driven H_2O_2 generation proceeded at a lower initial rate than under monochromatic light (~1.0 mmol L^{-1} h^{-1}) and the H_2O_2 concentration plateaued at 7.8 ± 1.4 mmol L^{-1} (3.3 ± 0.6 μmol cm^{-2}) after 10 h (Fig. S15a), reaching a steady state concentration as a result of the trade-off between photocatalytic ORR and H_2O_2 decomposition.[8] Using smaller volumes of solvents to increase the volume/interfacial surface area only had a marginal improvement in H_2O_2 concentration (Fig. S15b). Interestingly, using solar light concentrated with a magnifying Fresnel lens to increase the intensity up to 7 sun (~700 mW cm^{-2}) did not result in a significant enhancement of H_2O_2 from ORR or glyceraldehyde from GOR (Fig. S15c).

The low steady-state concentration of H_2O_2 achievable under the given conditions provides an additional benefit for the optimal activity of the enzyme iCALB. The lipase is known to suffer from deactivation at super-stoichiometric H_2O_2 concentrations (>30 wt%) typically adopted to achieve high substrate conversion. For that reason, previous reports worked around this drawback by slow, controlled addition of H_2O_2 to the reaction flask.[39,41] To assess the effect of H_2O_2 concentration on lipase deactivation, we compared the specific catalytic activity of iCALB in the esterification of propyl laurate (expressed as Propyl Laurate Units, or $\mu mol_{propyl\ laurate}$ min^{-1} $g^{-1}{}_{iCALB}$, see Supplementary Methods for the details) recovered after 24 h incubation at 37 °C in aqueous H_2O_2 at different concentrations. The activity of the enzyme recovered from a mixture of 10 mM H_2O_2 and 100 mM H_2O_2 was 6.3 ± 1.9 PLU to 1.5 ± 0.3 PLU, respectively (Fig. S16), illustrating the advantage of *in situ* H_2O_2 production to naturally maintain low local H_2O_2 concentrations to prevent enzymatic damage.

Nevertheless, the concentration of H_2O_2 produced under AM1.5G irradiation (7.8 ± 1.4 mmol L^{-1} in the bulk) was sufficient to initiate the domino catalysis. We therefore assessed the rise in epoxide content in the organic phase and the residual H_2O_2 in the aqueous phase generated within 4 h. Tests were run with 3 mL of 30 wt% aqueous glycerol, 50 mg of floatable H-CN_x/PP, 40 mg iCALB, 3 mL of 40 wt% oleic acid with saturated O_2 (1 atm) under mild orbital shaking (100 rpm) and room temperature. Due to natural aerobic oxidation, untreated oleic acid contained a small amount of epoxide (1.0 ± 0.1 μmol cm^{-2}, 2.4 ± 0.3 mmol L^{-1}). Nevertheless, the epoxide content more than doubled (2.5 ± 0.1 μmol cm^{-2}, 5.8 ± 0.2 mmol L^{-1}) within 4 h irradiation (Fig. 3a). Residual H_2O_2 reached a high of 0.8 ± 0.2 μmol cm^{-2} (2.0 ± 0.6 mmol L^{-1}), which was lower than the amount detected in the absence of organic substrate within the same reaction time (2.8 ± 0.4 μmol cm^{-2}, 6.5 ± 0.9 mmol L^{-1}, Fig. S15a) indicating the participation of *in situ* generated H_2O_2 to the enzymatic epoxidation catalysis.

Fractionation of vegetable oils for byproducts valorization

The greatest benefit of the multiphasic domino photocatalytic strategy proposed in this work is the possibility to use waste or byproduct streams as a single source for the biphasic liquid components of the system. Unsaturated fatty acids and glycerol can be both obtained from the biodiesel synthesis from vegetable oils through a transesterification reaction of unsaturated triglycerides with methanol followed by fractionation. We utilize both glycerol and the unreacted fatty acids that inevitably remain in the glycerol phase from their incomplete conversion into fatty acid methyl esters. To demonstrate the real-world applicability of this strategy, samples of vegetable oils were collected from local markets and kitchens, and samples of tall oils as an additional byproduct source for fatty acids valorization were received from a kraft pulp processing industrial facility (Fig. S17).

Following a typical protocol for biodiesel synthesis,[30] vegetable oils including rapeseed, sunflower, olive, soybean, and palm (~40 mL) were first reacted with methanol (9.8 mL, 242 mmol) and NaOH (410 mg, 10.3 mmol) under reflux for 1 h. After cooling to room temperature and allowing for spontaneous phase separation (Fig. 1a), the upper biodiesel fraction was collected and analyzed by gas chromatography-mass spectrometry (GC-MS) (Table S11). The glycerol phase was collected and acidified to pH ~ 2 with 85 wt% aqueous

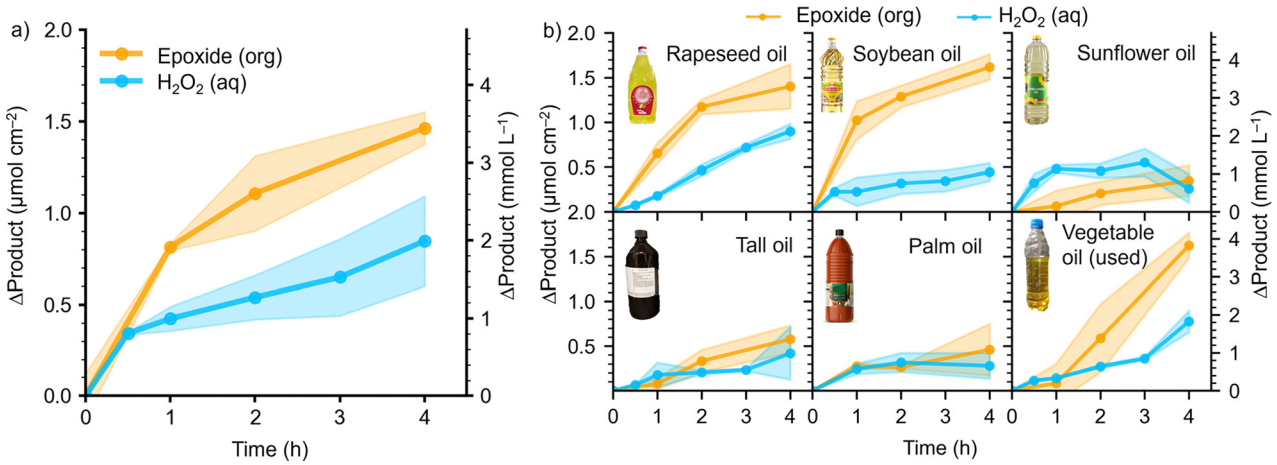

Fig. 3 Kinetics of production of epoxidized fatty acids (organic phase) and residual H_2O_2 (aqueous phase) under simulated solar light with (a) commercial pure glycerol and oleic acid and (b) glycerol and fatty acids extracted from vegetable or tall oils. Reaction conditions: aqueous glycerol (30 wt%, 3 mL), fatty waste diluted in ethyl acetate (3 mL), H-CN_x/PP (50 mg), iCALB (40 mg), AM1.5G (100 mW cm^{-2}, 1 sun), O_2 (1 atm), rt. Glycerol extracted from the respective fatty acid source was used for tests with fatty waste. Glycerol from used vegetable oil was used for tests with tall oil. Fatty waste was diluted in ethyl acetate to achieve a final concentration of total unsaturated fatty acids of ~40 wt%. The data are presented as mean values ± standard deviation (shadowed areas) for reactions performed in triplicate (n = 3).

phosphoric acid. Protonation of the unreacted fatty acids resulted in spontaneous partition from glycerol in a liquid phase of lower density (Fig. 1a). The upper phase was collected and washed with deionized water. The residual glycerol phase was washed with ethyl acetate, collected, and water was removed under reduced pressure. A scaled-up biodiesel synthesis and fractionation was performed using waste cooking oil (1 kg) from a local kitchen (Fig. S18). Fractions recovered from each oil (Fig. S19–S21) are summarized in Table 1. Glycerol, fatty acids and biodiesel were obtained with a yield of 5–12 wt%, 3–10 wt%, and 14–55 wt%, respectively. Residual soap, accounting for the rest of the mass balance, was discarded (Table S12).

Full valorization of fatty waste

Tests under AM1.5G irradiation were replicated with unsaturated fatty acids and glycerol extracted from vegetable oils. To demonstrate the concept of full valorization of fatty waste from a single source, in each experiment the glycerol and the fatty acids fraction from the same real-world sample were utilized. Phosphoric acid in the glycerol fraction was first neutralized with NaOH, buffering the pH around 7. Thus, the solution was diluted with water to a final glycerol content of approximately 30 wt%. The fatty acid fraction was diluted to an approximate concentration of 40 wt% of total unsaturated fatty acids (oleic + linoleic) based on the composition found in Table 2. Epoxide functionalities in the organic phase were detected and quantified by ^{1}H-NMR analysis for all vegetable oils and tall oils samples (Fig. S21). The epoxide concentration increased with irradiation to more than double the initial amount for all vegetable oils examined, with a Δepoxide from a low of 0.58 ± 0.15 μmol cm^{-2} (1.4 ± 0.4 mmol L^{-1}) from sunflower oil to a high of 1.6 ± 0.1 μmol cm^{-2} (3.8 ± 0.3 mmol L^{-1}) from used cooking oil.

Sylfat® tall oil was also assessed as a possible byproduct for the synthesis of epoxidized fatty acids. Sylvatal® was instead deemed less suitable for its lower content of unsaturated fatty acids and higher contaminations with abietic acid and other diterpenoids (Table 2). Interestingly, epoxidation of tall oils did not proceed to the same extent as for vegetable oils, with a marginal Δepoxide of 0.3 ± 0.2 μmol cm^{-2} (0.8 ± 0.4 mmol L^{-1}). The result could be attributed to unidentified organic substrates (including rosin acids, diterpenoids and unsaponifiable components such as sterols,

Table 2 Composition of unreacted fatty acids fraction extracted from vegetable oils in Table 1 and of tall oil samples

	Content (wt%)							
Fatty acid	Rapeseed	Sunflower	Olive	Soybean	Sylfat (Tall oil)	Sylvatal (Tall oil)	Palm	Used vegetable oil
Palmitic (16 : 0)	4.1	5.8	13.8	5.3	0.0	0.0	35.9	7.8
Stearic (18 : 0)	1.3	2.3	1.6	2.5	1.2	0.6	12.9	3.3
Oleic (18 : 1, *cis*-Δ^9)	46.6	30.3	52.0	32.7	36.4	22.9	29.8	42.9
Linoleic (18 : 2, *cis*,*cis*-Δ^9 Δ^{11})	43.0	42.8	13.6	46.2	51.7	25.5	15.5	57.2
Other fatty acids	<1.0	0.0	20.4	4.6	4.8	3.9	0.0	0.0
Other organic compounds[a]	0.0	0.0	0.0	0.0	0.0	>5%	0.0	0.0

[a] Abietic acid and structurally related compounds.

tocopherols) competing for oxidation or inaccurate ^{1}H-NMR quantification (Fig. S21). Palm oil was included to demonstrate the applicability of the concept to vegetable oils richer in saturated fatty acids. Incidentally, palm oil might be a particularly suitable choice for its on-site valorization, given its production is concentrated in equatorial or tropical countries including Malaysia, Indonesia, and Nigeria, benefiting from a higher annual solar irradiance.[52,53]

Overall, the results introduce L|S|L for domino photochemoenzymatic epoxidation as a sustainable, heterogeneous, macroscopically phase-segregated platform for the full valorization of fatty waste.

Scaled up, outdoor, and flow L|S|L domino photocatalysis

To investigate further the applicability of the compartmentalized reactor, we scaled up the reaction to a 100 mL volume scale for each liquid phase. Given the importance of the interfacial area between the immiscible phases, a large reactor ($\varnothing$ = 18 cm, total volume: 1.5 L, Fig. S22a) was used and filled with amounts of aqueous and organic phases to match the volume/surface ratio of smaller scale experiments (0.42 cm). The reactor was charged with 104 mL of 30 wt% aqueous glycerol and 104 mL 40 wt% oleic acid in ethyl acetate to replicate the same volume to surface ratio tested in small scale reactors (0.40 mL cm^{-2}), 1.8 g of H-CN$_x$/PP, 1.4 g of iCALB, sealed with a transparent lid, saturated with O_2 (1 atm), and irradiated from the top with AM1.5G irradiation. To improve mass transfer over the larger area, the reaction was conducted under mild stirring (100 rpm). Every 4 h, the organic and aqueous phases were sampled, and the reactor was purged with O_2 to maintain a saturated headspace.

After 48 h, epoxidized oleic acid rose in the organic phase from 1.0 ± 0.1 μmol cm^{-2} (2.4 ± 0.3 mmol L^{-1}) to 5.8 ± 0.7 μmol cm^{-2} (14.1 ± 1.7 mmol L^{-1}, Δepoxide = 4.8 ± 0.7 μmol cm^{-2} or 11.7 ± 1.7 mmol L^{-1}) (Fig. 4a). In the aqueous phase, glyceraldehyde was the major GOR product (92% selectivity), growing up to 28.9 ± 6.2 μmol cm^{-2} (70.8 ± 15.0 mmol L^{-1}), while dihydroxyacetone reached a high of 2.4 ± 1.7 μmol cm^{-2} (5.9 ± 4.0 mmol L^{-1}). The residual aqueous H_2O_2 (0.4 ± 0.2 μmol cm^{-2}, 1.0 ± 0.4 mmol L^{-1}) was negligible compared to the amount of GOR products. Incidentally, the temperature in the reactor rose to ∼40 °C in just two hours due to solar heating (Fig. S22b), which is within the ideal range for optimal iCALB activation (Fig. 2b) and did not vary significantly after 2 days of continuous irradiation. The mixture recovered from the large-scale reactor exhibited a very good phase separation, with both the floatable catalyst and the immobilized lipase sitting at the interface between the two liquid phases (Fig. S22c).

The emerging concept of macroscopic segregation of two immiscible liquids and a solid catalyst layer opens engineering opportunities not accessible with state-of-the-art nanoconfined reactors (*e.g.* micelles, liposomes). Most crucial is the possibility to operate on both liquid phases continuously and independently without the need for separation processes and with no loss of catalyst. Such degree of freedom is not allowed by equivalent multiphasic systems extensively based on emulsions.[10,11] Phase-segregated L|S|L systems therefore represent the optimal platform for operation in flow.

Continuous supply and extraction of both liquid phases – in mono-current (flow of only one liquid phase), co-current, or counter-current (double flow) mode – acquires particular significance for multiphasic domino reactions. Indeed, under simulated solar light and with mild orbital shaking, we observed a halt in epoxidation yield under prolonged reaction time (20 h, Fig. S23a). Instead, we observed a sustained generation of epoxide when the aqueous glycerol phase was semi-continuously replaced to reset the H_2O_2 concentration at the interface before its dilution in the whole volume of the aqueous layer (Fig. S23b). A detailed discussion of the experimental evidence is reported in Supplementary Note 3. We attribute this limitation to the levelling of *in situ* produced H_2O_2 concentration combined with its diffusion to the bulk of the aqueous phase, where it cannot participate as a substrate for the enzymatic step of the domino catalysis. To validate this hypothesis, we run finite element studies to simulate the distribution of H_2O_2 at the interface and in the bulk under batch and semi-continuous operation (Supplementary Notes 4, 5, Fig. S24, S25, Tables S13, S14 and Videos S1, S2).

The observed benefit of semi-continuous *vs.* batch modes becomes even more pronounced under continuous operation. Hence, we designed a custom flow photoreactor for chemical reactions in a L|S|L system (Fig. 4b). The reactor was fabricated in ultra-high molecular weight polyethylene (UHMWPE), and consisted of a main reaction chamber, two inlets and two outlets on opposite sides of the main unit for the transfer of organic and aqueous phases, a glass lid for top-down irradiation, a lateral port for gas purging, and a side viewing port. We tested the flow photoreactor under top-down AM1.5G irradiation in co-current mode. The aqueous glycerol phase was recirculated from a reservoir at different flow rates, while the organic phase was added dropwise at a constant flow rate of 0.25 mL min^{-1} and collected from the outlet by gravity (Fig. 4c and Fig. S26, Video S3).

Within 3 h irradiation, aqueous and organic products were generated at concentrations comparable to those achieved in small scale tests under monochromatic irradiation (Fig. 1d and 4d). The glyceraldehyde concentration in the aqueous reservoir reached a high of 19.1 ± 0.6 mmol L^{-1} at 1.0 mL min^{-1} flow rate. The drop at higher flow rates could be explained by a mismatch between the timescale of product extraction and diffusion from the interface, where the aqueous phase is not sufficiently enriched with the glycerol oxidation products before leaving the reactor. A similar trade-off was also confirmed by finite element simulations showing that excessive flow rates in a planar L|S|L reactor prevents accumulation in the bulk of the product generated at the interface (Fig. S27). It must be noted that the solid catalytic layer at the liquid–liquid boundary poses relevant engineering challenges compared to existing reactors for liquid–liquid extraction. For example, the occurrence of fouling, that is particle accumulation on the walls of the reaction chamber, especially after drainage, will have to receive special consideration in future studies on scaled-up

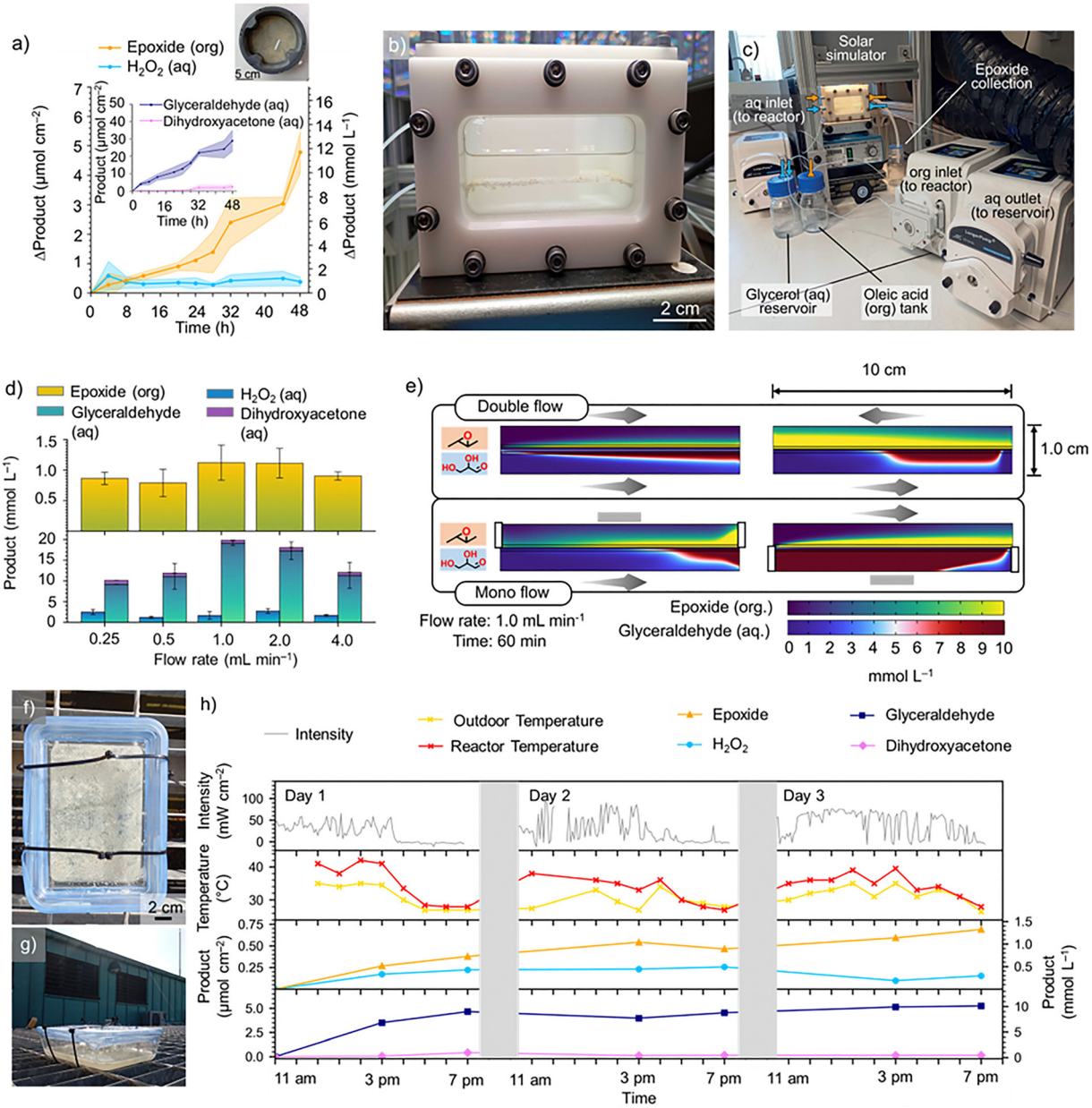

Fig. 4 (a) Kinetics of production of epoxidized oleic acid (organic phase), glyceraldehyde and dihydroxyacetone (aqueous phase) and residual H_2O_2 (aqueous phase) in a pilot-scale batch reactor (∅ = 18 cm). Reaction conditions: aqueous glycerol (30 wt%, 104 mL), oleic acid in ethyl acetate (40 wt%, 104 mL), H-CN_x/PP (1.8 g), iCALB (1.4 g), O_2 (1 atm), AM1.5G (100 mW cm^{-2}, 1 sun), rt. O_2 was bubbled for at least 5 min every 4 h. (b) Picture of the flow L|S|L photoreactor. (c) Picture of setup for photochemo-enzymatic catalysis in a flow L|S|L reactor. (d) Organic and aqueous products collected respectively in the outlet and reservoir of the flow photoreactor setup showed in c, at different flow rates. Reaction conditions: aqueous glycerol (30 wt%, 60 mL), oleic acid in ethyl acetate (40 wt%, 60 mL), H-CN_x/PP (500 mg), iCALB (400 mg), O_2 (1 atm), AM1.5G (100 mW cm^{-2}, 1 sun), rt. O_2 was bubbled for at least 5 min every 1 h. (e) Simulated epoxide and glyceraldehyde concentration profiles in a planar flow L|S|L reactor under different flow modes. (f) Top view of the glass box photoreactor used for tests under natural sunlight. (g) Glass box photoreactor installed on the rooftop of the Department of Chemistry of the University of Cambridge. (h) Domino photochemo-enzymatic epoxidation of oleic acid under natural sunlight in a planar batch reactor (16 × 12 × 5 cm) over 3 consecutive days. The data are presented as mean values ± standard deviation (error bars and shadowed areas) for reactions performed in triplicate (n= 3).

(meter-scale) flow reactors. Our custom flow reactor highlights the benefit of reactive and catalytic phases compartmentalization, that enables simultaneous seamless operation of all components with no disturbance of the catalytic layer. Future studies in scaled-up flow reactors will have to consider the proper handling of a solid catalytic layer

Finite element simulations allow to visualize the operation of a planar flow L|S|L photoreactor (Fig. 4e) under different flow modes. Calculations show that epoxide generation would particularly benefit from a double flow counter-current operation, for better utilization of *in situ* generated H_2O_2, while a mono flow of the organic phase was the best configuration for

glyceraldehyde production, where the GOR product accumulates in the bottom layer and is not diluted by an inlet aqueous flow (Fig. 4e and Fig. S27–S30).

Finally, to demonstrate the applicability of the system to a real-world scenario, we executed the photochemo-enzymatic reaction outdoors under natural sunlight over 3 consecutive days (Fig. 4f–h). The tests were run in a transparent glass box charged with 100 mL 30 wt% aqueous glycerol, 100 mL of 40 wt% oleic acid in ethyl acetate, 1.4 g H-CN_x and 1.0 g iCALB (Fig. S31). The box was purged every hour with O_2. In the brightest hours of the day (between 1 and 3 pm) the temperature in the reactor rose above 40 °C due to solar heat, favoring enzymatic activity. Both the epoxide and glyceraldehyde in the aqueous phase were produced continuously over 3 days, up to 0.69 μmol cm^{-2} (1.3 mmol L^{-1}) and 5.3 μmol cm^{-2} (10.1 mmol L^{-1}), respectively.

Comparative life cycle assessment and simplified techno-economic analysis

To investigate the benefit of an integrated, solar-driven system for the full valorization of byproducts from the biodiesel

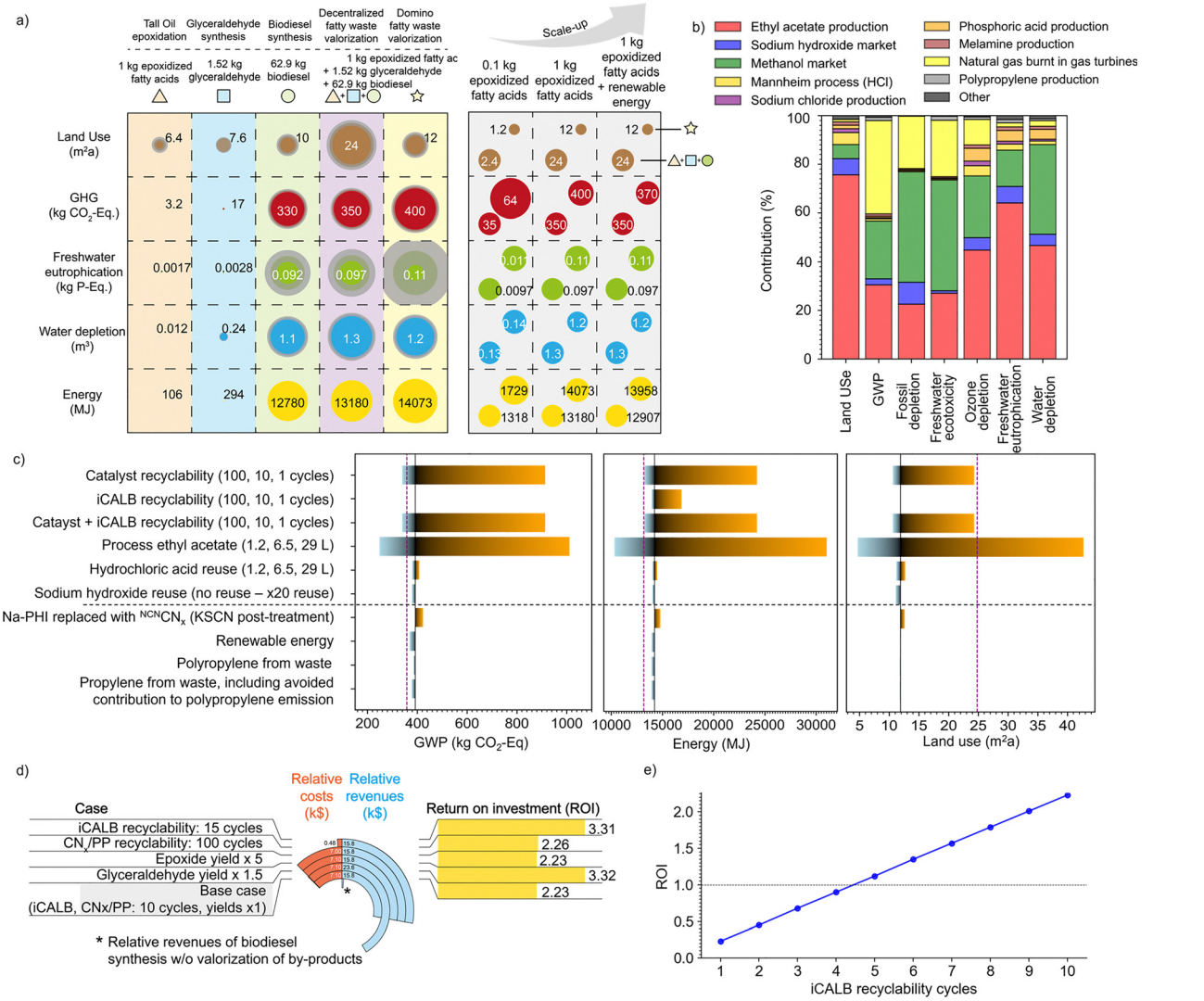

Fig. 5 (a) Environmental impact analysis results for individual processes of decentralized fatty waste valorization (tall oil epoxidation, glyceraldehyde synthesis, biodiesel synthesis), their total, and for integrated photocatalytic domino valorization of fatty waste. The area of the bubbles and gray areas indicate the computed average values and the corresponding standard deviations. The cumulative energy distribution computation tool does not have uncertainty capabilities. (b) Environmental impact hotspot analysis of integrated photocatalytic domino valorization of fatty waste. (c) Sensitivity analysis of integrated photocatalytic domino valorization of fatty waste on global greenhouse emissions, energy use, and land use. The effects of continuous variables (above horizontal dotted line) and point variables (below horizontal dotted line) are shown. For continuous variables, values for optimistic, base, and pessimistic cases are reported in brackets on the left. The vertical purple dotted line indicates the total environmental impact of the decentralized fatty waste valorization (tall oil epoxidation + glyceraldehyde synthesis + biodiesel synthesis). (d) Comparative techno-economic sensitivity analysis. Reported costs and revenues are for the process of integrated domino valorization of fatty waste relative to a conventional biodiesel synthesis process where fatty acids and glycerol are discarded as byproducts. ROI is calculated as the ratio between relative costs and revenues. The revenues from selling fatty waste and glycerol from the conventional biodiesel synthesis process are indicated with an asterisk. (e) ROI calculated as in (d) as a function of iCALB recyclability cycles.

synthesis, we conducted a comparative cradle-to-gate life cycle impact assessment (LCIA) of our integrated, domino process and a set of independent, decentralized processes targeting the synthesis of biodiesel, epoxidized fatty acids from tall oil, and glyceraldehyde from glycerol (Fig. S32–S35 and Tables S15–S19). For a proper comparison, we assessed the impact of three separate processes producing the same amount of products obtained in our work, and extrapolated the results for the production of 1 kg of epoxidized fatty acids,[54,55] 1.53 kg glyceraldehyde,[56] and 62.9 kg of biodiesel.[30]

LCIA analysis reveals that the domino process leads to a significantly lower impact compared to the decentralized production on land use (12 ± 2 *vs.* 24 ± 3 m^2a) and a marginal improvement on water depletion (1.2 ± 0.1 m^3 *vs.* 1.3 ± 0.1 m^3) (Fig. 5a and Tables S20–S23). Although the domino process at this stage exhibits a higher global warming potential (GWP) than the decentralized due to the low epoxidation yields and the high input from electricity production needed for catalyst synthesis (Fig. 5b), the difference in impact can be attenuated at larger scales. Assuming the energy needed for the synthesis of the catalyst is largely independent on the produced amount, the GWP difference between the integrated and decentralized process decreases by 69% scaling up from 100 g to 1 kg of epoxidized fatty acids, and it is further reduced by 9% when electricity for the catalyst synthesis is sourced from renewables (Fig. 5a).

A sensitivity analysis (Tables S24 and S25) reveals that the domino process results in 5.1% lower GWP than the decentralized production in an optimistic scenario allowing for the reuse of both H-CN_x/PP and iCALB over 100 cycles of 48 h continuous irradiation (Fig. 5c). As highlighted by the hotspot analysis (Fig. 5b), recycling ethyl acetate is an even more impactful measure to improve the environmental feasibility of our method. If the organic solvent is recycled or its use in washing is minimized, the GWP and energy use of our method are mitigated to 69% and 78% of the decentralized production, respectively.

Finally, we run a simplified comparative techno-economic analysis to illustrate the economic advantage of integrated biodiesel synthesis and byproducts valorization. We compared the relative costs and revenues of a biodiesel synthesis plant outsourcing glycerol and unreacted fatty acids to third parties, and a plant including solar-driven upcycling of the byproducts into glyceraldehyde and epoxidized fatty acids. Glyceraldehyde production generates the highest share of revenues (Tables S26 and S27), while costs are largely determined by the immobilized enzyme iCALB (Table S28). On a base case, assuming an iCALB recyclability over 10 runs of 48 h continuous irradiation, integrated full valorization of fatty waste results in a relative return on investment (ROI) of 2.2, that can increase to 19.3 with a recyclability over 100 runs, and to 11.0 with a 5-fold increase in glyceraldehyde yield (Fig. 5d and Table S29). As the relative costs of the domino process are dominated by the floatable enzyme, the calculated ROI has a seemingly linear dependence on the number of iCALB recyclability cycles (Fig. 5e and Fig. S36). Our analysis forecasts that 5 recyclability cycles are sufficient to bring the relative ROI above the economic feasibility threshold (1.1) (Fig. 5e).

Given the relatively low economic asset of epoxidized fatty acids and oils (2.8 \$ kg^{-1}),[57,58] which are instead precursors to more valuable polymers and plasticizers,[27,28] we recommend that the solar-driven domino epoxidation can generate even higher revenues pivoting to low-cost organic substrates that can be converted in reactive intermediates for fine chemical synthesis.

Conclusions

We designed a macroscopic phase-segregated L|S|L system combining spontaneous product separation and domino aqueous-organic chemical conversion driven by sustainable solar light, a floatable metal-free, safe, inexpensive photocatalyst, and a floatable commercially available immobilized enzyme. The photochemo-enzymatic domino catalysis proceeds through light-driven glycerol oxidation coupled with H_2O_2 evolution photocatalyzed by polymeric carbon nitride, and *in situ* H_2O_2 utilization for lipase-catalyzed alkene epoxidation in a water-immiscible organic phase.

The multi-phasic system was applied for the paired synthesis of hydrophobic epoxidized fatty acids and hydrophilic glyceraldehyde and dihydroxyacetone, demonstrated excellent robustness over 10 consecutive domino catalytic cycles, with an average of 0.62 ± 0.12 μmol cm^{-2} *cis*-8,9-epoxystearic acid and 4.6 ± 0.3 μmol cm^{-2} glyceraldehyde produced. The system leverages on significant synergies for enzymatic activity: the slow release of H_2O_2 by *in situ* production mitigates lipase deactivation, and the optimal temperature for enzymatic activation (40 °C) can be achieved by solar heating. Isotopic labelling confirmed the multi-step oxygen atom transfer from atmospheric O_2 to the epoxide ring. The proposed reactor design also provides an excellent strategy for the full valorization of fatty waste beyond biodiesel synthesis, targeting the upcycling of glycerol and unreacted fatty acids, which are usually considered byproducts. The concept was demonstrated sourcing both glycerol and fatty acids from vegetable oil and tall oil samples collected from a local kitchen and a Kraft pulp industry, respectively.

Chemical substrates supplied from byproducts and the low cost of materials needed for catalyst preparation suggest the potential for large scale operation of the phase-segregated reactor, which we illustrated with a 100 mL-scale batch photoreactor under simulated AM1.5G (5.8 ± 0.7 μmol cm^{-2} epoxide and 28.9 ± 6.2 μmol cm^{-2} glyceraldehyde in 48 h), and natural sunlight irradiation (0.69 μmol cm^{-2} epoxide and 5.3 μmol cm^{-2} glyceraldehyde over 3 consecutive days). A comparative life cycle assessment and simplified techno-economic analysis suggests that the photocatalytic integrated domino valorization has a lower overall environmental impact than the decentralized valorization of the byproducts from the biodiesel synthesis, with an optimized floating catalyst recyclability over 100 runs, or with optimized product yields achievable with

careful reactor design. Finally, we also demonstrated the unique benefit of macroscopic L|S|L compartmentalization in a flow reactor for continuous collection of the liquid phases and mitigation of limitations imposed by mass transfer. This work moves the emerging field of floatable photocatalysis at the liquid–liquid interface from simple chemical compartmentalization to multi-phasic domino synthesis.

Experimental section

Materials

Melamine (99%, Sigma-Aldrich), potassium thiocyanate (98%, Alfa Aesar), sodium chloride (≥99.5%, Fischer Scientific), potassium chloride (Fischer Scientific), cyanamide (ChemCruz), cyanuric acid (99%, Alfa Aesar), lithium chloride (Sigma Aldrich), ammonium chloride (Breckland Scientific Supplies), potassium iodide (99%, Breckland Scientific Supplies), hydrochloric acid (~37%, Fisher Scientific), sulfuric acid (≥ 95%, Fisher Scientific), hydrogen peroxide (100 volumes, > 30% w/v, Fisher Scientific), O_2 (BOC), $^{18}O_2$ (97 atom%, Sigma-Aldrich), potassium titanium oxide oxalate dihydrate (Sigma-Aldrich), polypropylene (PP, amorphous, Aldrich), *cis*-cyclooctene (95% stab., Thermo Scientific), cyclooctene oxide (99%, Sigma Aldrich), glycerol (≥99%, Sigma Aldrich), oleic acid (technical grade, 90%, Aldrich), lipase acrylic resin from *Candida antarctica* (5000 U g^{-1} recombinant, expressed in *Aspergillus niger*, Sigma Aldrich), Lipase B *Candida antarctica*, recombinant from *Aspergillus oryzae* (9 U mg^{-1}, Sigma Aldrich), dihydroxyacetone (Merck), DL-glyceraldehyde (≥90%, Sigma), lauric acid (99.5%, Thermo Scientific), 1-propanol (Breckland Scientific Supplies), propyl dodecanoate (MedChem), palmitic acid (≥98%, Sigma Aldrich), oleic acid (≥99%, Sigma Aldrich), linoleic acid (ChemCruz), arachidic acid (≥99%, Sigma Aldrich), phenolphthalein (98.5%, Thermo Scientific), phenyltrimethylammonium hydroxide (0.1 M in methanol, Thermo Scientific) were used without further purification. Rapeseed oil, sunflower oil, and olive oil were purchased by Sainsbury's. Soybean oil was purchased by Thermo Scientific. Samples of tall oil (Sylfat™, Sylvatal™) were kindly provided by Kraton™. Palm oil was purchased by Supelco Sigma Aldrich. Waste vegetable oil was kindly provided by Hughes Hall College at University of Cambridge.

Synthetic procedures

Synthesis of cyanamide-functionalized polymeric carbon nitride (K-CN_x). Following a previously reported procedure,[59] melamine (5 g) was heated at 550 °C for three hours (temperature ramp 1 °C min^{-1}) under air in a crucible with a lid. The yellow powder was mixed with potassium thiocyanate (weight ratio 1 : 2) and the mixture was heated at 400 °C for 1 h and then at 500 °C for 30 min (ramp rate 30 °C min^{-1}) under Ar in a ceramic boat in a tube furnace.[60] The powder was allowed to cool down to room temperature, washed with water (25 mL × 2) and with ethanol (25 mL), and dried overnight at 65 °C.

Synthesis of protonated cyanamide-functionalised CN_x (H-CN_x). Protonated cyanamide-functionalised CN_x was prepared according to a reported procedure.[34] 2 mL of 37 wt% aqueous HCl were added to 200 mg of K-CN_x in a 15 mL centrifuge tube. The tube was immediately vortexed and shaken. The sample was centrifuged (11 000 rpm, 10 min), the supernatant discarded and washed with MilliQ water (5 × 40 mL). Finally, the sample was dried overnight at 65 °C.

Fabrication of floatable composites (CN_x/PP). Following a previously reported procedure,[8] amorphous polypropylene pellets were first cooled down in liquid N_2 and immediately ground with a commercial coffee grinder. Fine particles were then separated through a commercial sieve (80 mesh). K-CN_x or H-CN_x and plastic powders in 6 : 4 w/w ratio were transferred to a mortar. Liquid N_2 was poured on the CN_x-plastic mixture before grinding to ensure that the plastic was sufficiently brittle to yield a uniform solid mixture. The powder mixture was ground and transferred into a round-bottomed flask. The solid blend was stirred for 30 min with no solvent at 122 °C. Water was added to the flask and the floating fraction was separated in a separatory funnel and washed several times with MilliQ water. The solid was dried overnight at 65 °C.

Characterization

A TESCAN MIRA3 field emission gun-scanning electron microscope equipped with an Oxford Instruments Aztec Energy X-maxN 80 EDX system was used for Scanning Electron Microscopy (SEM) and Energy-Dispersive X-Ray (EDX) analysis. UV-Vis spectra were recorded on an Agilent Cary 60 equipped with a Harrick Scientific Video Barrelino probe for analysis in diffuse reflectance mode. Attenuated total reflection-infrared (ATR-IR) spectroscopy was performed on a Thermo-Scientific Nicolet iS50. Thermogravimetric analysis (TGA) was performed on a Mettler Toledo TGA/DSC 2 Star System under N_2 (100 mL min^{-1}). X-Ray photoelectron spectroscopy (XPS) analysis was performed using a Thermo Scientific Escalab 250Xi fitted with a monochromated Al Kα X-ray source (1486.7 eV). All data were recorded with an X-ray beam size of 650 μm, a pass energy of 20 eV at a step size of 0.1 eV. Electronic charge neutralization was achieved using an ion source. Ion gun current = 100 μA. Ion gun voltage = 40 V. All sample data were recorded at a pressure below 10^{-8} Torr and a room temperature of 294 K. Ultraviolet photoemission spectroscopy (UPS) analysis was performed using Thermo Scientific Escalab 250Xi fitted with a Helium lamp producing a He I (21.2 eV) source. Contact angle measurements were performed dropping deionized water on samples spray-coated (~300 μm thickness) on glass slides from 20 mg mL^{-1} suspensions in ethanol. LC-MS data were acquired using a MSE method in negative ionization modes in a Waters VION QTOF instrument, equipped with a UPLC inlet using a Waters BEH 1.7 μM C18 column in a water:acetonitrile gradient and 0.1% formic acid. The injection volume was 5 μL, capillary voltage was set to 0.7 kV, collision energy for the low energy channel was kept at 6 eV and the high energy channel was ramped from 15 to 45 eV. Lock mass correction was applied over the run. Source

temperature was set to 120 °C and desolvation temperature to 280 °C, while cone gas flow was 50 L h^{-1} and desolvation gas flow was kept at 800 L h^{-1}.

Fractionation of fatty waste

Samples of cooking oil or tall oil were first treated for the synthesis of biodiesel according to a reported protocol.[30] In a typical procedure, a 100 mL round-bottomed flask was charged with 40 mL vegetable oil, 9.8 mL methanol (242 mmol), 410 mg NaOH (10.3 mmol). The mixture was heated to reflux under stirring for 1 h. After cooling down, the phases were allowed to separate in a separatory funnel. The biodiesel fraction (top) was isolated, while the glycerol phase (bottom) was washed with ethyl acetate (3 × 10 mL). Soap (sodium carboxylates) precipitating as a white pulp was discarded. After washing, the glycerol phase was diluted with ~20 mL MilliQ water and acidified with aqueous ortophosphoric acid (85 wt%) until pH ~2. The mixture was allowed to separate into an orange fraction of fatty acids on top and a cloudy colorless fraction of glycerol at the bottom. The phases were allowed to separate in a separatory funnel. Fatty acids were extracted with ethyl acetate (3 × 5 mL) and the solvent was removed under reduced pressure. Water in the glycerol phase was removed at 50 °C under reduced pressure (80 mbar).

Catalytic tests

Optimization of photocatalytic H_2O_2 production. In a typical test, 2 mL of aqueous glycerol, 5 mg of catalyst, were added to a glass vial (∅ = 2 cm, total volume: 11.5 mL). The vial was sealed with a crimp-cap and a rubber septum, and the mixture was purged with O_2 for 2 min. The vial was irradiated with a blue LED (450 nm, 40 ± 4 mW cm^{-2}) at 25 °C for 1 h under 250 rpm orbital shaking. For catalyst screening, a glycerol concentration of 50 wt% was used. For glycerol concentration screening, H-CN_x was used as the catalyst.

Optimization of enzymatic oleic acid epoxidation. In a typical test, 2 mL of 40 mM aqueous H_2O_2, 2 mL of 40 wt% oleic acid in ethyl acetate, and 40 mg of iCALB were added to a glass vial (∅ = 2 cm, total volume: 11.5 mL). The vial was sealed with a crimp-cap and a rubber septum and shaken at 250 rpm at 25 °C for 16 h. Deviations from these parameters were chosen accordingly for the optimization of temperature, iCALB loading and organic solvent.

Domino photochemo-enzymatic epoxidation and recyclability. In a typical test, 2 mL of 30 wt% aqueous glycerol, 2 mL of 40 wt% oleic acid in ethyl acetate, 20 mg of H-CN_x/PP, and 40 mg of iCALB were added to a glass vial (∅ = 2 cm, total volume: 11.5 mL). The vial was sealed with a crimp-cap and a rubber septum, and the mixture was purged with O_2 for 2 min. The vial was irradiated with a blue LED (450 nm, 40 ± 4 mW cm^{-2}) at 25 °C for 1 h under 250 rpm orbital shaking. For recyclability tests, after this time the aqueous and organic phases were sampled for analysis, removed with a syringe with needle, and replaced with fresh aqueous glycerol and oleic acid in ethyl acetate. The fresh solutions were added slowly to allow CN_x/PP and iCALB to float at the liquid–liquid interface. The mixture was purged with O_2 and irradiated again, repeating the procedure for 10 consecutive runs.

Domino photochemo-enzymatic epoxidation of unsaturated fatty acids from cooking oil and tall oil under simulated sunlight. In a typical test, 3 mL of 30 wt% aqueous glycerol, 3 mL of ~40 wt% unsaturated fatty acids in ethyl acetate, 50 mg of H-CN_x/PP, and 40 mg of iCALB were added to a custom glass reactor for top-down irradiation (∅ = 3 cm, total volume: 50 mL, Fig. 1c). The reactor was sealed with a screwcap and a rubber septum, purged with O_2 for 5 min, and irradiated with a G2V Sunbrick LED Solar Simulator (AM1.5G, 100 mW cm^{-2}) for 4 h under 100 rpm orbital shaking, periodically sampling the organic and aqueous phase. A 400 nm cutoff filter was placed at the top of the photoreactor to prevent UV-driven H_2O_2 decomposition. In tests with commercial-grade chemicals, pure glycerol and oleic acid diluted in MilliQ water and ethyl acetate, respectively, were used. In tests for the valorization of byproducts from cooking oils, the glycerol and unsaturated fatty acid phases recovered from oil fractionation and diluted in MilliQ water and ethyl acetate, respectively, were used. For tall oil, the glycerol phase extracted from waste vegetable oil and diluted in water was used.

For experiments with concentrated solar light, solar concentration was achieved on a Newport LOT-QD LS0816-H large area solar simulator using a Xe lamp by focusing simulated AM1.5G solar light with a commercial Fresnel lens (XL Full Page, 3× magnification, PVC). A front surface SiO_2-protected 8″ square aluminum mirror (Thorlabs) was used to deflect light from the solar simulator to the top of the photoreactor. The light intensity was set to 3 to 7 sun (300–700 mW cm^{-2}) and measured with a Newport 843-R optical power meter, adjusting the distance between the lens and the photoreactor.

For large (100 mL) scale experiments, a custom cylindrical reactor (∅ = 18 cm, total volume: 1.5 L), equipped with a screwable transparent plastic lid was charged with 104 mL of 30 wt% glycerol, 104 mL of 40 wt% oleic acid in ethyl acetate, 1.8 g H-CN_x/PP, and 1.4 g iCALB. The reactor was purged with O_2 and irradiated under mild stirring (100 rpm) with a G2V Sunbrick LED Solar Simulator (AM1.5G). The aqueous and organic phases were sampled periodically for 48 h, and O_2 was purged after every sampling.

For experiments in flow photoreactor, a custom ultra-high molecular weight polyethylene (UHMWPE) reactor (7.3 × 7.3 cm, total volume: 230 mL) comprising one inlet and one outlet for each liquid phase, a side window for viewing purposes, a glass lid and a screwable window cap (Fig. 4b,c and Fig. S26) was charged with 60 mL 30 wt% aqueous glycerol, 60 mL of 40 wt% oleic acid in ethyl acetate, 500 mg H-CN_x/PP, and 400 mg iCALB. The reactor was purged with O_2 before the reaction and every hour. The aqueous phase was circulated from a reservoir of 22.5 mL of 30 wt% aqueous glycerol with peristaltic pumps (LongerPump, BT100-3J) at different flow rates. Fresh 40 wt% oleic acid in ethyl acetate was flowed into the upper organic phase of the reactor with a peristaltic pump (LongerPump, BT100-3J) at a flow rate of approximately 0.25 mL min^{-1}. The reactor was irradiated with a G2V Sunbrick

LED Solar Simulator (AM1.5G) under mild stirring (100 rpm) for 3 h. The organic outlet was collected by gravity into a separate bottle. After the reaction, epoxidized oleic acid was quantified in the collected organic phase, H_2O_2 and glycerol oxidation products were quantified in the aqueous reservoir.

For experiments outdoors with natural sunlight irradiation, a Pyrex glass box (16 × 12 × 5 cm, total volume: 0.8 L) with a glass lid was charged with 100 mL of 30 wt% glycerol, 100 mL of 40 wt% oleic acid in ethyl acetate, 1.4 g H-CN_x/PP, and 1.0 g iCALB. The box was placed on the rooftop of the Department of Chemistry of the University of Cambridge for three consecutive days, from the 13th to the 15th August 2025. Every day from 9 am to 7 pm, every hour the box was purged with O_2, and temperature outside and inside the box was recorded with a thermometer. Light intensity was logged with a Newport 843-R optical power meter. The aqueous and organic phases were sampled at 3 pm and 7 pm every day.

Isotopic labelling

2 mL of 30 wt% aqueous glycerol, 2 mL of 40 wt% oleic acid in ethyl acetate, 20 mg H-CN_x/PP, and 40 mg iCALB were added to a glass vial (∅ = 2 cm, total volume: 11.5 mL). The vial was sealed with a crimp-cap and a rubber septum. In separate tests, the vial was either purged with natural-abundance O_2 for 2 minutes or vacuumed and refilled with a slight overpressure (~1.2 atm) of $^{18}O_2$ (97 atom%). The vial was irradiated with a blue LED (450 nm, 40 ± 4 mW cm^{-2}) at 25 °C for 1 h under 250 rpm orbital shaking, followed by orbital shaking at 250 rpm at 37 °C in the dark for 16 h. The organic phase was analyzed by LC-MS as described in the characterization section above.

Product analysis

H_2O_2 in the aqueous phase was quantified by the titanium(IV) oxalate colorimetric method,[35] using a 10 g L^{-1} aqueous solution of titanium oxide oxalate dihydrate ($K_2[TiO(C_2O_4)_2]\cdot 2H_2O$) in concentrated sulfuric acid as the color-evolving reactant and reading the absorbance at 400 nm. Calibration curves were made with external standards (Fig. S37).

Glyceraldehyde and dihydroxyacetone from glycerol oxidation were quantified by high-performance liquid chromatography (HPLC) with external standards (Fig. S37) on a Waters Breeze system equipped with refractive index (RID-2414) and diode array UV–vis (λ = 210 and 254 nm) detectors using an Ion-Exclusion ROA-Organic Acid H+ (8%) column at 70 °C. Samples were analyzed in the isocratic flow mode (flow rate 1.0 mL min^{-1}, 0.005 M H_2SO_4 HPLC water).

Cyclooctene oxide from *cis*-cyclooctene oxidation was quantified by gas chromatography equipped with a flame ionization detector (GC-FID) with decane as the internal standard (Fig. S37). Samples were analyzed on a Shimadzu QP2020 (EI) instrument equipped with an SH-I-5MS column (length: 30 m, inner diameter: 0.25 mm, film thickness: 0.25 μm) with He as the carrier gas at a flow rate of 1 mL min^{-1} (oven temperature segment 1: 60.0 °C, hold time 1.0 min, segment 2: ramp rate 30 °C min^{-1}, hold time 3.67 min, injection temperature: 250.0 °C, detector temperature: 280.0 °C, H_2 flow: 40 mL min^{-1}, air flow: 400 mL min^{-1}).

Epoxidized unsaturated fatty acids were quantified by ^{1}H-NMR spectroscopy (Bruker Neo Prodigy 400 MHz) in $CDCl_3$ from the multiplet at 2.90 ppm, using 1,3,5-trimethoxybenzene as the internal standard.

Propyl laurate was quantified by gas chromatography equipped with a flame ionization detector (GC-FID) using decane as the internal standard (Fig. S37). Samples were analyzed on an Agilent 8890 GC System coupled with a 5977C GC/MSD detector instrument equipped with a HP-5MS-UI column (length: 30 m, inner diameter: 0.25 mm, film thickness: 0.25 μm) with N_2 as the carrier gas at a flow rate of 1 mL min^{-1} (oven temperature segment 1: 80.0 °C, hold time 2.0 min, segment 2: ramp rate 20 °C min^{-1}, 200 °C, hold time 3.0 min, segment 3: ramp rate 20 °C min^{-1}, 250 °C, hold time 2 min, injection temperature: 250 °C, detector temperature: 380 °C, H_2 flow: 40 mL min^{-1}, air flow: 400 mL min^{-1}). For tests to assess the activity of iCALB recovered from mixtures at different concentrations of aqueous H_2O_2, propyl laurate was quantified by a calibration curve made with external standards (Fig. S37).

The composition of the fatty acid fractions extracted from samples of vegetable oils and tall oil was determined by GC-FID according to the standard method ASTM D5974-20.[61] GC operating conditions were as above, except for the injection temperature, that was raised to 300 °C for *in situ* methylation of the fatty acids. The ester composition of the biodiesel fraction was determined by GC-FID analysis with the standard conditions listed above.

Finite element modelling

Finite element method (FEM) simulations were performed using COMSOL Multiphysics Software.[62] Simulations were run to investigate the effect of periodical replacement of the aqueous phase (semi-continuous operation) on the average interfacial H_2O_2 concentration and the rate of epoxidation in the organic phase, and the amounts of products extracted from the organic and aqueous phase under continuous operation with different flow modes (mono current, double co-current, double counter-current) and flow rates. Full details are available in Supplementary Notes 4 and 5.

Life cycle assessment and techno-economic analysis

A comparative life cycle impact assessment (LCIA) of the integrated fatty waste valorization reported in this work and a hypothetical decentralized valorization consisting of individual biodiesel synthesis, glyceraldehyde synthesis, and fatty acids epoxidation was conducted on OpenLCA with the Ecoinvent v3.8 database and the ReCiPe Midpoint – H method.[63,64] A simplified techno-economic analysis was conducted to compare the economic benefit of the reported domino protocol for *in-situ* byproduct valorization in biodiesel synthesis as opposed to a traditional biodiesel plant with byproduct sold to third parties. Full details are available in Supplementary Note 6.

Conflicts of interest

There are no conflicts to declare.

Data availability

The data that support the findings of this study are available from the University of Cambridge data repository: https://doi.org/10.17863/CAM.129346. The data supporting this article have been included as part of the supplementary information (SI). Supplementary information: supplementary Notes 1–6, supplementary Fig. 1–37, supplementary Tables 1–27. See DOI: https://doi.org/10.1039/d5ee07523h.

Acknowledgements

We gratefully acknowledge support by the Cambridge Trust (PhD scholarship to A.R.), UK Research and Innovation (EP/S022953/1 to A.R., ERC Advanced Grant EP/X030563/1 to E.R.), UK Department of Science, Innovation and Technology and the Royal Academy of Engineering Chair in Emerging Technologies program (CIET-2324-83 to E. R.). The XPS and UPS data collection was supported by the Henry Royce Institute for advanced materials through the Equipment Access Scheme enabling access to the Royce XPS facility at Cambridge; Cambridge Royce Facilities grant EP/P024947/1 and Sir Henry Royce Institute – recurrent grant EP/R00661X/1. The authors would like to acknowledge Dr Heather Greer for assistance with electron microscopy, Natalie Potter and the Melville Lab for assistance with contact angle analysis, Dongseok Kim for assistance with zeta potential measurements, and Flora Mammadova and Prof. Pawel Dydio for assistance with GC-MS analysis. The authors would also like to thank Dr Zhipeng Huang and Papa Kwarteng for helpful discussion.

References

1 S. Linley, C. Pornrungroj and E. Reisner, Floating solar technologies for sustainable chemical synthesis on open water, *Nat. Chem. Eng.*, 2026, **3**, 34–46.
2 C. Pornrungroj, A. B. Mohamad Annuar, Q. Wang, M. Rahaman, S. Bhattacharjee, V. Andrei and E. Reisner, *Nat. Water*, 2023, **1**, 952–960.
3 S. Linley and E. Reisner, *Adv. Sci.*, 2023, **10**, 2207314.
4 W. H. Lee, C. W. Lee, G. D. Cha, B.-H. Lee, J. H. Jeong, H. Park, J. Heo, M. S. Bootharaju, S.-H. Sunwoo, J. H. Kim, K. H. Ahn, D.-H. Kim and T. Hyeon, *Nat. Nanotechnol.*, 2023, **18**, 754–762.
5 W. H. Lee, H. Park, C. W. Lee, H. Kim, J. H. Jeong, J. I. Yun, S.-U. Bang, J. Heo, K. H. Ahn, G. D. Cha, M. S. Bootharaju, B.-H. Lee, J. Ryu, M. Kim, T. Hyeon and D.-H. Kim, *Nat. Nanotechnol.*, 2025, **20**, 1237–1246.
6 Y. Xie, M. Wang, Q. Huang, Q. Huang, B. Sheng, W. Song, H. Sheng and J. Zhao, *Energy Environ. Sci.*, 2024, **17**, 4725–4734.
7 Z. Zhang, Y. Wang, Y. Xie, T. Tsukamoto, Q. Zhao, Q. Huang, X. Huang, B. Zhang, W. Song, C. Chen, H. Sheng and J. Zhao, *Nat. Commun.*, 2025, **16**, 274.
8 A. Rogolino, S. Linley, P. K. Kwarteng, S. Bonke, C. Pulignani and E. Reisner, *Chem*, 2025, 102827.
9 L. Velasco-Garcia and C. Casadevall, *Commun. Chem.*, 2023, **6**, 263.
10 S. Rodríguez-Jiménez, H. Song, E. Lam, D. Wright, A. Pannwitz, S. A. Bonke, J. J. Baumberg, S. Bonnet, L. Hammarström and E. Reisner, *J. Am. Chem. Soc.*, 2022, **144**, 9399–9412.
11 H. Zhang, J. Jaenecke, I. L. Bishara-Robertson, C. Casadevall, H. J. Redman, M. Winkler, G. Berggren, N. Plumeré, J. N. Butt, E. Reisner and L. J. C. Jeuken, *J. Am. Chem. Soc.*, 2024, **146**, 34260–34264.
12 S.-y Takizawa, T. Okuyama, S. Yamazaki, K.-i Sato, H. Masai, T. Iwai, S. Murata and J. Terao, *J. Am. Chem. Soc.*, 2023, **145**, 15049–15053.
13 M. Pera-Titus, L. Leclercq, J.-M. Clacens, F. De Campo and V. Nardello-Rataj, *Angew. Chem., Int. Ed.*, 2015, **54**, 2006–2021.
14 P. Gaudin, R. Jacquot, P. Marion, Y. Pouilloux and F. Jérôme, *ChemSusChem*, 2011, **4**, 719–722.
15 P. A. Zapata, J. Faria, M. P. Ruiz, R. E. Jentoft and D. E. Resasco, *J. Am. Chem. Soc.*, 2012, **134**, 8570–8578.
16 L. Leclercq, A. Mouret, A. Proust, V. Schmitt, P. Bauduin, J.-M. Aubry and V. Nardello-Rataj, *Chem. - Eur. J.*, 2012, **18**, 14352–14358.
17 C. Wu, S. Bai, M. B. Ansorge-Schumacher and D. Wang, *Adv. Mater.*, 2011, **23**, 5694–5699.
18 S. Rodríguez-Jiménez, E. Lam, S. Bhattacharjee and E. Reisner, *Green Chem.*, 2023, **25**, 10611–10621.
19 Y. Zhang, Q. Cao, A. Meng, X. Wu, Y. Xiao, C. Su and Q. Zhang, *Adv. Mater.*, 2023, **35**, 2306831.
20 F. He, Y. Lu, Y. Wu, S. Wang, Y. Zhang, P. Dong, Y. Wang, C. Zhao, S. Wang, J. Zhang and S. Wang, *Adv. Mater.*, 2023, **36**, 2307490.
21 L.-L. Liu, F. Chen, J.-H. Wu, J.-J. Chen and H.-Q. Yu, *Proc. Natl. Acad. Sci. U. S. A.*, 2023, **120**, e2215305120.
22 C. Ortiz, M. L. Ferreira, O. Barbosa, J. C. S. dos Santos, R. C. Rodrigues, Á. Berenguer-Murcia, L. E. Briand and R. Fernandez-Lafuente, *Catal. Sci. Technol.*, 2019, **9**, 2380–2420.
23 A. F. Aguilera, P. Lindroos, J. Rahkila, M. M. Klimov, P. Tolvanen and T. Salmi, *Chem. Eng. Process.*, 2022, **174**, 108882.
24 W. Wikström, A. Freites Aguilera, P. Tolvanen, R. Lassfolk, A. Medina, K. Eränen and T. Salmi, *Ind. Eng. Chem. Res.*, 2023, **62**, 9169–9187.
25 H. Greim, in *Encyclopedia of Toxicology*, ed. P. Wexler, Academic Press, Oxford, 2024, 4th edn, pp. 1003–1006.
26 M. Garone, J. Howard and J. Fabrikant, *J. Clin. Aesthet. Dermatol.*, 2015, **8**, 43–47.
27 R. Chen, C. Zhang and M. R. Kessler, *J. Appl. Polym. Sci.*, 2015, 132.
28 S. Caillol, M. Desroches, G. Boutevin, C. Loubat, R. Auvergne and B. Boutevin, *Eur. J. Lipid Sci. Technol.*, 2012, **114**, 1447–1459.

29 G. Papps and D. F. Othmer, *Ind. Eng. Chem.*, 1944, **36**, 430–434.
30 J. Yang, C. Xu, B. Li, G. Ren and L. Wang, *J. Chem. Educ.*, 2013, **90**, 1362–1364.
31 H. Hou, X. Zeng and X. Zhang, *Angew. Chem., Int. Ed.*, 2020, **59**, 17356–17376.
32 X. Fang, X. Huang, Q. Hu, B. Li, C. Hu, B. Ma and Y. Ding, *Chem. Commun.*, 2024, **60**, 5354–5368.
33 Z. Chen, A. Savateev, S. Pronkin, V. Papaefthimiou, C. Wolff, M. G. Willinger, E. Willinger, D. Neher, M. Antonietti and D. Dontsova, *Adv. Mater.*, 2017, **29**, 1700555.
34 A. Rogolino, I. F. Silva, N. V. Tarakina, M. A. R. da Silva, G. F. S. R. Rocha, M. Antonietti and I. F. Teixeira, *ACS Appl. Mater. Interfaces*, 2022, **14**, 49820–49829.
35 R. M. Sellers, *Analyst*, 1980, **105**, 950–954.
36 E. M. Roth and E. S. Shanley, *Ind. Eng. Chem.*, 1953, **45**, 2343–2349.
37 W. D. Nicoll and A. F. Smith, *Ind. Eng. Chem.*, 1955, **47**, 2548–2554.
38 T. Cogliano, V. Russo, R. Turco, E. Santacesaria, M. Di Serio, T. Salmi and R. Tesser, *Chem. Eng. Sci.*, 2022, **251**, 117488.
39 E. G. Ankudey, H. F. Olivo and T. L. Peeples, *Green Chem.*, 2006, **8**, 923–926.
40 Y. Xu, N. R. B. J. Khaw and Z. Li, *Green Chem.*, 2009, **11**, 2047–2051.
41 L. Yu, C. Zou, Q. Li, Z. Liu, Y. Liu and A. Tang, *Bioprocess Biosyst. Eng.*, 2023, **46**, 1331–1340.
42 C. Aouf, E. Durand, J. Lecomte, M.-C. Figueroa-Espinoza, E. Dubreucq, H. Fulcrand and P. Villeneuve, *Green Chem.*, 2014, **16**, 1740–1754.
43 S. Warwel and M. Rüschgen Klaas, *J. Mol. Catal. B:Enzym.*, 1995, **1**, 29–35.
44 U. Törnvall, C. Orellana-Coca, R. Hatti-Kaul and D. Adlercreutz, *Enzyme Microb. Technol.*, 2007, **40**, 447–451.
45 Q. Wang, C. Pornrungroj, S. Linley and E. Reisner, *Nat. Energy*, 2022, **7**, 13–24.
46 M. A. Bajada, A. Vijeta, A. Savateev, G. Zhang, D. Howe and E. Reisner, *ACS Appl. Mater. Interfaces*, 2020, **12**, 8176–8182.
47 Q. Wang, J. Warnan, S. Rodríguez-Jiménez, J. J. Leung, S. Kalathil, V. Andrei, K. Domen and E. Reisner, *Nat. Energy*, 2020, **5**, 703–710.
48 T. Uekert, M. A. Bajada, T. Schubert, C. M. Pichler and E. Reisner, *ChemSusChem*, 2021, **14**, 4190–4197.
49 S. Mazzanti, G. Manfredi, A. J. Barker, M. Antonietti, A. Savateev and P. Giusto, *ACS Catal.*, 2021, **11**, 11109–11116.
50 S. Ranganathan, T. Gärtner, L. O. Wiemann and V. Sieber, *J. Mol. Catal. B: Enzym.*, 2015, **114**, 72–76.
51 T. Nishimi, T. Kamachi, K. Kato, T. Kato and K. Yoshizawa, *Eur. J. Org. Chem.*, 2011, 4113–4120.
52 Y. Basiron, *Eur. J. Lipid Sci. Technol.*, 2007, **109**, 289–295.
53 H. Soon Min, A. Lomi, E. Okoroigwe and L. Rodríguez-Urrego, *Int. J. Renew. Energy Res.*, 2019, **9**, 86–95.
54 E. A. Bried, Epoxidation of tall oil fatty acids and esters, US3207743A, United States, 1963.
55 FMC Corp, Epoxidation of fatty acids, GB772151A, United Kingdom, 1967.
56 K. Zoltán, *J. Chem. Res.*, 2024, **48**, 17475198231226386.
57 Oleic Acid, Sigma-Aldrich. Available at: https://www.sigmaaldrich.com/GB/en/substance/oleicacid28246112801 (Accessed: March 2026).
58 Epoxidized Soybean Oil (ESO/ESBO), alibaba.com. Available at: https://www.alibaba.com/product-detail/Epoxidized-Soybean-Oil-ESO-ESBO-CAS_1600546177783.html (Accessed: March 2026).
59 J. Liu, Y. Liu, N. Liu, Y. Han, X. Zhang, H. Huang, Y. Lifshitz, S.-T. Lee, J. Zhong and Z. Kang, *Science*, 2015, **347**, 970–974.
60 V. W.-h Lau, I. Moudrakovski, T. Botari, S. Weinberger, M. B. Mesch, V. Duppel, J. Senker, V. Blum and B. V. Lotsch, *Nat. Commun.*, 2016, **7**, 12165.
61 D5974-20, A. Standard Test Methods for Fatty and Rosin Acids in Tall Oil Fractionation Products by Capillary Gas Chromatography, ASTM D5974-20, ASTM International, 2020.
62 COMSOL Multiphysics® v. 6.3. https://www.comsol.com. COMSOL AB, Stockholm, Sweden.
63 OpenLCA, https://www.openlca.org, GreenDelta, GmbH, Berlin, Germany.
64 The ecoinvent Database, Version 3.8: https://www.ecoinvent.org; Zürich: ecoinvent.